JACS
JOURNAL OF THE AMERICAN CHEMICAL SOCIETY

ARTICLE

pubs.acs.org/JACS

Measuring the Partitioning Kinetics of Membrane Biomolecules Using Patterned Two-Phase Coexistant Lipid Bilayers

Ling Chao and Susan Daniel*

Department of Chemical and Biomolecular Engineering, Cornell University, Ithaca, New York 14853, United States

Supporting Information

ABSTRACT: We report a new method for measuring the partitioning kinetics of membrane biomolecules to different lipid phases using a patterned supported lipid bilayer (SLB) platform composed of liquid-ordered (lipid raft) and liquid-disordered (unsaturated lipid-rich) coexistent phases. This new approach removes the challenges in measuring partitioning kinetics using current in vitro methods due to their lack of spatial and temporal control of where phase separation occurs and when target biomolecules meet those phases. The laminar flow configuration inside a microfluidic channel allows us to pattern SLBs with coexistent phases in predetermined locations and thus eliminates the need for additional components to label the phases. Using a hydrodynamic force provided by the bulk flow in the microchannel, target membrane-bound species to be assayed can be transported in the bilayers. The predefined location of stably coexistent phases, in addition to the controllable movement of the target species, allows us to control and monitor when and where the target molecules approach or leave different lipid phases. Using this approach with appropriate experimental designs, we obtain the association and dissociation kinetic parameters for three membrane-bound species, including the glycolipid G_{M1}, an important cell signaling molecule. We examine two different versions of G_{M1} and conclude that structural differences between them impact the kinetics of association of these molecules to raft-like phases. We also discuss the possibilities and limitations for this method. One possible extension is measuring the partitioning kinetics of other glycolipids or lipid-linked proteins with posttranslational modifications to provide insight into how structural factors, membrane compositions, and environmental factors influence dynamic partitioning.

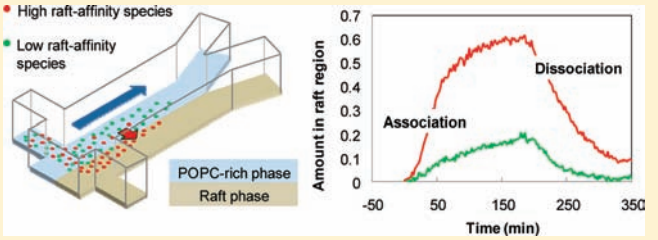

INTRODUCTION

Current understanding of the cell membrane suggests that it is a patchwork structure composed of multiple proteins and lipids that are not all freely diffusing and well-mixed, but rather can take part in dynamic microdomains.[1−8] Separation of distinct lipid membrane domains within the cell membrane has been suggested to play important roles in many cellular processes by providing various microenvironments to cluster or to isolate membrane biomolecules.[1,8,9] One class of liquid-ordered membrane domain, enriched in sphingolipids and cholesterol, is called a lipid raft.[9−11] Under specific conditions, certain glycolipids, proteins, and other membrane species exhibit a high affinity for lipid rafts; while other species prefer the more disordered phase surrounding the rafts.[7,12,13] Identification of critical lipid−protein interactions and changes in affinity of certain biomolecules with lipid raft phases may be critical to understanding the causes of a number of diseases, including infertility,[14] viral infection and associated diseases,[15] Alzheimer's disease,[16] and other age-related diseases[17,18] and is therefore vital for designing the most effective therapeutic drugs to combat these diseases.

At the moment, there are limited approaches to identify and classify the affinity of membrane biomolecules to different lipid domains. Current in vivo methods attempt to characterize the residency of membrane molecules to various lipid phases using detergent and/or high salt/alkaline pH to isolate insoluble membrane fractions and then correlate the contents of those fractions.[3,5] However, these assorted chemicals and conditions lead to variations in compositions from experiment to experiment and often contamination with species from other cellular compartments, which compromises the reliability of this approach. Other strategies to identify microdomain residents involve the direct labeling of the intact cell membrane;[5,19] however, surface labeling of cells requires antibodies, toxins, or nanoscale beads to bind to specific species, which can cross-link them and cause artifactual enrichment.[20−22] In contrast to these methods, some in vitro methods incorporate target species into model membranes such as giant plasma vesicles,[23,24] giant unilamellar vesicles,[25,26] or supported lipid bilayers[12,27,28] to study their partition behavior in carefully controlled conditions. These approaches report the affinity of membrane biomolecules to different lipid domains by their partition coefficients, defined as the detected concentration distribution of the target molecules among the different phases.[29] Because the first detection time point occurs long after the molecules have been exposed to the various lipid phases, the partitioning process already begins, or even completes, during the preparation step; therefore, the kinetics of the partitioning process are often missed.

Received: June 11, 2011
Published: August 17, 2011

However, information about the kinetics of the partitioning process is especially important and relevant to our understanding of membrane organization and function because cells are not in equilibrium,[8,10,13] and species are dynamically entering and leaving various regions within the cell membrane. The current understanding of cell membrane lipid rafts is that they are highly dynamic and transient, and they can sometimes be stabilized to form large microdomains.[10,11,30] How fast a biomolecule can partition into the membrane domain compared to the lifetime of the domain, the kinetic competition of various molecules for a particular microdomain, and the time scale of their association with different phases relative to the time scale of particular biological events are all important to correctly predict cell responses and the regulation of protein activity.[31,32] In the special case of membrane-bound species, recent literature highlights the importance of considering not only structure as a determining factor for membrane protein function but also the coupling of protein dynamics and the interaction with the local lipid environment.[31] For a membrane molecule to associate with a patch of lipid domain, it may need to diffuse to the patch, pass across the interface, and diffuse inside the patch. Current methods for studying the dynamic membrane heterogeneity such as single particle techniques and fluorescence correlation spectroscopy (FCS)[33] focus on obtaining the diffusion rate for a molecule in different specified phases or detecting the lifetime of the membrane domains. However, as far as we know, no method has been developed to study the rate of a membrane species passing across a phase interface between the coexistent phases. The challenge comes from the experimental difficulty in defining the phase interface and monitoring the species passing the well-defined interface.

To study the kinetics of a membrane biomolecule associating or dissociating from one membrane phase into another, one needs to critically determine when partitioning starts and monitor the concentration change in different phases in real time. Herein, we describe an enabling microfluidic platform for measuring association/dissociation kinetics that employs patterned lipid membrane phases at predefined locations. We control when membrane biomolecules meet or leave a particular lipid phase and thus can monitor partitioning from very early times. Using this new platform with appropriate experimental designs, we are able to measure the early time association/dissociation kinetics of membrane-bound species to/from different lipid phases and report the kinetic parameters for the partitioning of several membrane-bound species, including an important signaling glycolipid, G_{M1}.

Principle of the Method. Domain size and location are difficult to control in conventional model membrane systems, where an unpredictable phase separation process is used to generate membranes with two-phase coexisting regions.[25,34−37] Because phase separation and biomolecule partitioning are happening concurrently in this conventional approach, it is nearly impossible to track the biomolecule of interest to measure its association kinetics to a particular phase. In contrast to conventional methods, we first prepared the compositions of stable coexistent phases separately as vesicle solutions and then patterned them together to create a contiguous two-phase supported lipid bilayer within a microfluidic channel network. Supported lipid bilayers can be formed by lipid vesicle fusion inside microfluidics and have served as excellent mimics of the cell membrane in numerous applications in these platforms.[38−42] The choices for the two compositions that yield stable phase-separated bilayers are guided by tertiary lipid phase diagrams,[43,44] as described in the Supporting Information. The two-phase pattern is formed using laminar flow to deliver lipid vesicles of specific compositions to certain regions within the microfluidic channel.[45,46] Vesicles fuse, and the resulting bilayer regions heal together, but do not mix, to form a contiguous two-phase bilayer. Characterization of membrane phase stability is provided in the Supporting Information. Figure 1 illustrates the heterogeneous bilayer platform composed of stable, two-phase regions patterned in a striped arrangement inside a microfluidic channel (denoted by blue and tan colors). Biomolecules whose partitioning behavior we wish to assay are patterned in the "T" side channel. These molecules are denoted as red and green dots in the figure. The specific membrane-bound biomolecules to assay are fluorescently tagged to visualize and monitor their association with each lipid phase and track changes in their partitioning using a basic inverted fluorescence microscope. Because the locations of the two phases within the membrane are known, we do not require any special labeling of the phases themselves and therefore avoid any artifacts that could result from labeling. Then, we use a hydrodynamic force from the bulk flow (blue arrow) in the main microchannel to transport the membrane-bound biomolecules along the main channel where they contact the raft phase and can partition into it (red arrow). We emphasize that all transport and partitioning takes place within the two-dimensional supported bilayer plane where the two phases meet along a "line" interface. We conduct our experiments in a way so that the association kinetics and dissociation kinetics can be decoupled in our measurements and both the kinetic parameters can be obtained, as we will describe later.

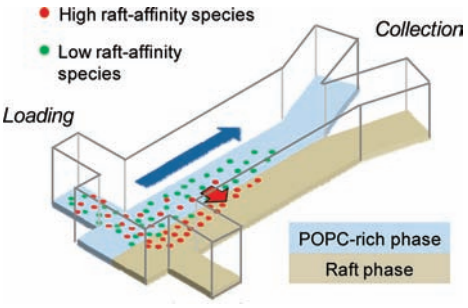

Figure 1. Illustration of a microfluidic device designed to measure kinetics of membrane-bound biomolecule partitioning. Laminar flow in a microfluidic channel is used to create stripes of lipid raft phase (brown) and POPC-rich phase (blue) in parallel along the main microchannel and to load a mixture of biomolecules to assay (red and green) in the side channel. The interface between the phases is contiguous, allowing molecules to diffuse across this interface and partition (red arrow) into the raft phase as they are transported down the main channel by hydrodynamic force from bulk buffer flow through the channel (blue arrow). Note that the membrane phases and loading bilayers are all adsorbed to the glass substrate on the channel bottom and the partitioning is taking place laterally within the two-dimensional plane of the bilayer.

EXPERIMENTAL SECTION

Materials. A detailed list of materials and suppliers is provided in the Supporting Information. Here we only provide a brief list of the materials used in this work. Lipids and additives used to make bilayers of various compositions were as follows: 1-palmitoyl-2- oleoyl-*sn*-glycero-3-phosphocholine (POPC), cholesterol (Chol), and *N*-palmitoyl-D-*erythro*-sphingosylphosphorylcholine (PSM). Three lipids were used in the

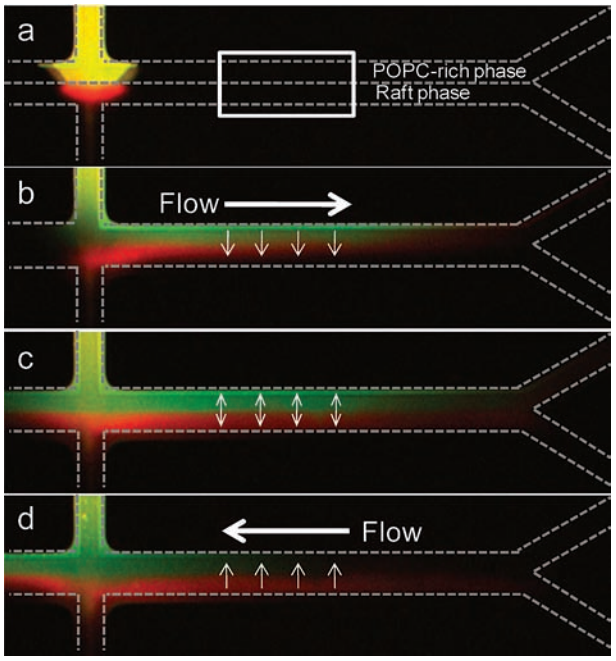

Figure 2. Left side: (a) A bird's eye view fluorescent image of the microfluidic device and loading bilayer containing red Alexa594-G_{M1} and green head-labeled BODIPY-DHPE. The POPC-rich phase is loaded in the top part of the main channel while the raft phase is in the bottom half. Both of these phases are initially devoid of any fluorophore; the interface between the phases and the boundary of the microchannel are marked by dashed lines that have been superimposed on the image. The white box in panel a is the control volume used for data analyses for kinetic measurements. The red color in the raft region close to the load shows that some of the red-labeled G_{M1} already started to partition into raft phase during the preparation step. Note that the penetration of the G_{M1} into this phase is more significant than into the POPC-rich phase at this time point because the raft and loading bilayers have had a longer contact time during the bilayer patterning steps (see Supporting Information for details). (b) Hydrodynamic force induced by the bulk flow in the microchannel is applied to the direction denoted by the large white arrow to move the mixed species originating in the side channel down the POPC-rich-phase membrane into the main chamber. An increasing amount of red G_{M1} is extracted into the raft phase with time during the transport. This is indicated by the smaller white arrows. (c) Eventually the hydrodynamic flow is stopped and the system is allowed to equilibrate for 2 h. Most of red G_{M1} partitions to the raft phase and most of green BODIPY-DHPE remains in the POPC-rich phase. (d) A hydrodynamic flow is applied in the opposite direction to move the target species back down the channel.

kinetic studies: *N*-(4,4-difluoro-5,7-dimethyl-4-bora-3a,4a-diaza-*s*-indacene-3-propionyl)-1,2-dihexadecanoyl-*sn*-glycero-3-phosphoethanolamine, triethylammonium salt (BODIPY FL DHPE), a headgroup-labeled lipid denoted as BODIPY-DHPE in this work; bovine brain asialoganglioside-G_{M1} labeled with Alexa Fluor 594 hydrazide, denoted here as head-labeled G_{M1}; BODIPYFL-C5 G_{M1}, denoted here as tail-labeled G_{M1}.

Methods. A detailed description of the methods used in this work is provided in the Supporting Information. This includes the following: procedure for labeling the headgroup of G_{M1}; bilayer composition selection, phase diagrams, and vesicle formation; description of the microfluidic device and its fabrication; patterning the coexistent bilayers within the microfluidic device; fluorescence intensity versus concentration for each biomolecule in each lipid phase; experimental setup; image processing; diffusion measurements; two-phase bilayer stability controls; kinetic data analysis.

RESULTS AND DISCUSSION

Formation of Contiguous Patterned Membrane and Loading and Transport of Membrane-Bound Biomolecules. We demonstrate the ability to form a contiguous patterned membrane and to transport membrane species in them using hydrodynamic flow of the aqueous buffer within the microfluidic channel, as captured in Figure 2. First, we formed a contiguous lipid membrane with POPC-rich phase (70/20/10 molar ratio of POPC/PSM/Chol), raft phase (60/40 molar ratio of PSM/Chol), and load membrane with 1 mol % of Alexa-594 head-labeled G_{M1} and 1 mol % of head-labeled BODIPY-DHPE doped in the POPC-rich phase. These two molecules are used for this demonstration because G_{M1} is well-known to have high affinity to raft, while BODIPY-DHPE associates with raft to a lesser extent.[28] The detailed formation procedure of the patterning heterogeneous membrane is provided in the Supporting Information. Here we just summarize the main features of the assay necessary to understand the kinetic analysis. Figure 2a shows the image after patterning the various bilayers in the device before a hydrodynamic force was applied to transport the species in the membrane. The yellow color indicates the mixture of both green BODIPY-DHPE and red Alexa-594 head-labeled G_{M1}. The red color close to the loading entrance shows that the membranes are connected, as Alexa-594 head-labeled G_{M1} is already able to diffuse and partition into the raft phase region in the membrane even before any flow has started.

In Figure 2b, an applied hydrodynamic flow of the bulk solution in the microchannel provides a shear stress to drive the lipid membrane on the glass support to move. The use of shear stress from hydrodynamic flow above supported bilayers to move membrane-bound species has been characterized and reported in the literature.[47] While other methods to transport molecules in supported bilayers are also available (e.g., electrophoresis), we chose hydrodynamic flow because we can utilize physiological buffers and are not limited to only assaying charged biomolecules. We measured that the fluorescently labeled species in the POPC-rich phase of our system move approximately ten times faster in the POPC-rich phase than they do in the raft phase under the same hydrodynamic flow conditions (Supporting Information). The relative speed difference between the two phases allows us to view the entire system as a 2-D process in a membrane plane where convective flow of the POPC-rich phase membrane passes the embedded target molecules along the interface of a relatively fixed raft phase. Figure 2c shows the partitioning after the hydrodynamic flow inside the microchannel was stopped for 2 h to allow molecules to penetrate into the raft phase region and reach equilibrium; here it is easy to see the distinct phases divided by a well-defined interface down the middle of the main channel.

Finally, when we induce hydrodynamic flow in the opposite direction, as shown in Figure 2d, we observed a convective flow moving the species in the opposite direction. In this image it is also easy to see that the species in the POPC-rich phase bilayer move much faster than those in the raft phase. When the flow is reversed, the POPC-rich phase enriched in BODIPY-DHPE (green) is transported back through the channel much faster than the G_{M1} (red) enriched in the raft phase, even though G_{M1} has a much larger extracellular structure extending into the bulk flow compared to BODIPY-DHPE (see structures in Figure 3c). A video of the time course of these steps is available in the Supporting Information.

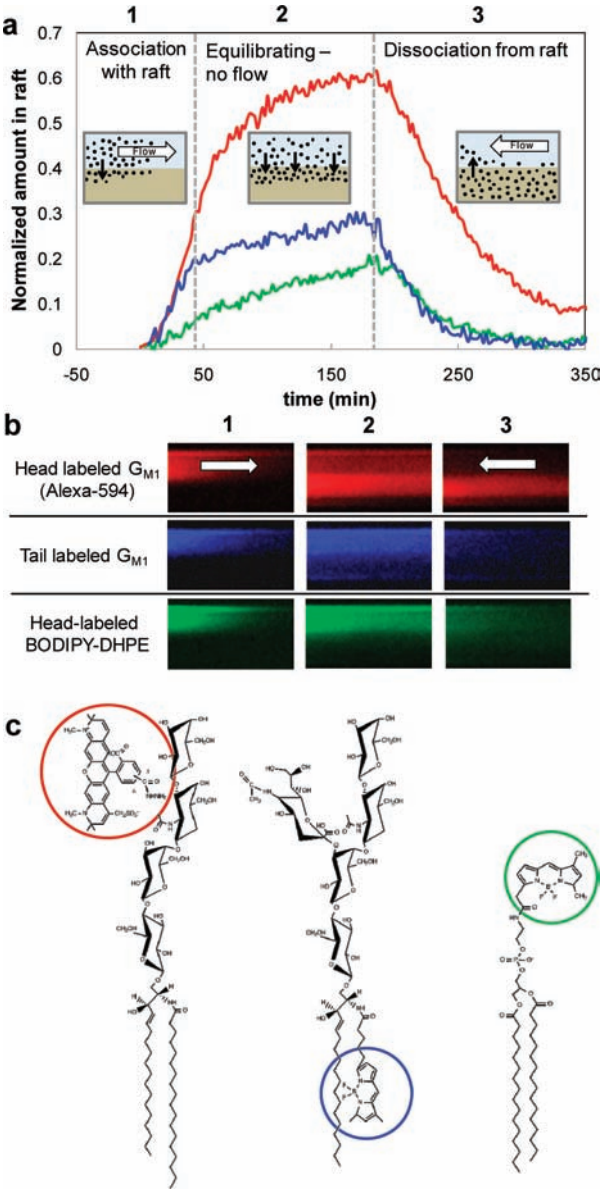

Figure 3. Partitioning kinetic measurement of Alex594-head-labeled G_{M1} (red), BODIPY-tail-labeled G_{M1} (blue, false color), and BODIPY-DHPE (green). (a) Species' content in the raft phase varying with time during the three stages: (1) flowing the species in the POPC-rich phase into contact with a fresh raft phase; (2) stopping the flow to let the system equilibrate; (3) applying reversed flow to allow the fresh POPC-rich phase to enter into the channel for the dissociation step. (b) Corresponding images at an arbitrary time point during the three different stages. These have been false-colored to match the line scan colors in the above plot. The temporal evolutions of the concentration profiles across the two phases at each stage are provided in the Supporting Information. (c) The chemical structures and labeling positions for head-labeled G_{M1}, tail-labeled G_{M1}, and BODIPY-DHPE.

Partitioning Kinetic Measurements by Monitoring Species Concentrations in the Raft Phase over Time. We next demonstrate how to use this platform to measure association/dissociation kinetics by monitoring species concentrations using fluorescence intensity as a proxy for concentration (see Supporting Information for characterization of the fluorescence intensity of each biomolecule in each phase). The partitioning assay is

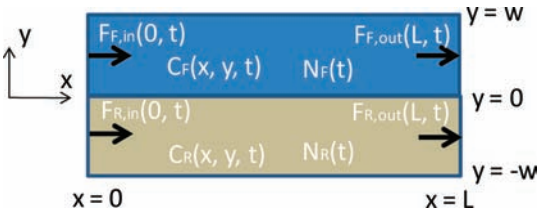

Figure 4. An illustration of the patterned membrane in the control volume for the mass balance calculation used to determine the target species' association or dissociation kinetic rate with a specific membrane phase. In this case, we examine the association and dissociation rates of G_{M1} and BODIPY-DHPE with the raft phase (in tan) from the POPC-rich phase (in blue). N_R is the amount of species in the raft phase region; L is the interface length between the raft phase and the POPC-rich phase $F_{R,in}$ and $F_{R,out}$ are the convective molar flow rates into and out the raft region. $F_{F,in}$ and $F_{F,out}$ are the convective molar flow rates into and out the POPC-rich region. w is the width of each phase. The subscripts "R" and "F" refer to the raft and POPC-rich phases, respectively.

carried out in three stages: association stage, equilibrium stage, and dissociation stage (Figure 3). The experimental procedure and analyses are somewhat analogous to the measurement of adsorption/desorption binding kinetics by surface plasmon resonance (SPR),[48] except here we are in a 2-D planar geometry and observing association/dissociation kinetics of membrane-bound biomolecules to/from a lipid membrane phase along an interface. To obtain association kinetics from POPC-rich phase to raft phase, target species in the POPC-rich phase were brought to a pristine raft phase and the amount entering into the raft phase in the control volume was monitored over time (Figure 3, stage 1).

After most of the species initially loaded in the channel entered into the main partitioning channel, the next step was to stop the convective flow and wait until the system equilibrated (Figure 3, stage 2). Equilibration was assumed when the concentration profile no longer changed significantly across the interfacial region (see Supporting Information for additional information). Finally, to obtain dissociation kinetics, the net amount of species leaving the raft phase was monitored when the hydrodynamic flow was reversed and fresh POPC-rich phase membrane could be monitored for the reassociation of molecules now moving from the raft phase back into the POPC-rich phase (Figure 3, stage 3). We tested three different molecules: Alex594-head-labeled G_{M1}, BODIPY-tail-labeled G_{M1}, and head-labeled BODIPY-DHPE. Figure 3a shows how their accumulation amount in the raft phase varies with time during the different stages, and Figure 3b shows a corresponding image observed during each of the association, equilibration, and dissociation stages. Figure 3c shows the chemical structures of the target biomolecules used in these studies.

Theory of Partitioning Kinetic Analyses. We analyzed the association/dissociation kinetics of fluorescently labeled species into/from the raft phase using a mass-balance approach. A control volume used for the mass balance is illustrated in Figure 4. The accumulation of species in the raft phase over time can be represented as:

$$\frac{dN_R}{dt} = \int_{x=0}^{x=L} r_+(C_F(x,0,t), k_+)dx - \int_{x=0}^{x=L} r_-(C_R(x,0,t), k_-)dx + (F_{R,in}(0,t) - F_{R,out}(L,t)) \quad (1)$$

where N_R is the amount of species in the raft phase region, L is the interface length between the raft phase and the POPC-rich

phase, r_+ is the association term, a function of species concentration at the interface in the POPC-rich phase ($C_F(x,0,t)$) and association rate constant (k_+), r_- is the dissociation term depending on the species concentration at the interface in the raft phase $C_R(x,0,t)$ and dissociation rate constant (k_-), and $F_{R,in}$ and $F_{R,out}$ are the convective molar flow rates into and out the raft region. The subscripts "R" and "F" refer to the raft and POPC-rich phases, respectively.

Association Kinetics Analysis. To obtain the association kinetics information from the POPC-rich phase to the raft phase, we operated our experiment in such a way so that only the association term, r_+, is important and the dissociation term and the convective flow rate terms can be neglected in eq 1. At the beginning of our experiment, we provided a hydrodynamic force to move the species into the control volume (the white box in Figure 2). The control volume is initially devoid of any fluorophores. We set the time for species entering into the POPC-rich phase region inside the control volume as time zero. When time was close to zero, $F_{R,in}$ and $F_{R,out}$ were still negligible because the species moved much faster (ten times) in the POPC-rich phase than in the raft phase. In addition, at a time close to zero, r_- was also negligible because the concentration in the raft phase was still very low. Next, we assumed that the association follows first-order kinetics in species concentration, so that eq 1 can be simplified to eq 2 at the beginning of the association stage:

$$\frac{dN_R(t)}{dt} = \int_{x=0}^{x=L} k_+ C_F(x,0,t)dx \qquad (2)$$

In the association stage, species concentration at the interface in the POPC-rich phase, $C_F(x,0,t)$, varied significantly with both x and t, and its integration over x and t is sensitive to the interface boundary we chose. To obtain a more robust way of expressing the integration term, we applied a mass balance for the POPC-rich phase region and replaced the integration term with a function of the inlet and outlet molar flow rates in the POPC-rich phase. Equation 2 can then be written as eq 3:

$$N_R(t_a) = \frac{k_+}{w}\int_{t=0}^{t=t_a}\left(\int_{t=0}^{t=t_a} F_{F,in}(0,t) - F_{F,out}(L,t)dt\right)dt \qquad (3)$$

where $F_{F,in}$ and $F_{F,out}$ are the convective molar flow rates into and out of the POPC-rich phase region, w is the width of the POPC-rich phase (as shown in Figure 4), and t_a is a certain time after the species started to enter into the control volume. To determine the association rate constant, k_+, from our data, we defined a parameter, α, in eq 3, and plotted the net amount of species in the raft phase (N_R) against α in Figure 5. α is defined as:

$$\alpha = 1/w\int_{t=0}^{t=t_a}\left(\int_{t=0}^{t=t_a} F_{F,in}(0,t) - F_{F,out}(L,t)dt\right)dt \qquad (4)$$

Note that because eq 3 is valid only at early times, when the dissociation term and convective flow terms in the raft phase (in eq 1) are still negligible, only the initial slope of the plot represents k_+.

Next, we check if the first-order kinetic assumption we made in the analysis is valid. When the kinetics are first order in concentration, the amount entering the raft depends on the summation of all of the species concentrations approaching the interface. On the other hand, if the kinetics are not first order, the amount entering into the raft phase will depend on the concentration distribution. For example, for a second-order association, a sharp concentration distribution along the two-phase interface causes a higher overall flux of species entering into the raft region than the one with a uniform concentration distribution, because the high concentration provides more weight because it is squared. Therefore, to check if the association kinetics are indeed first order with concentration, we varied the initial species concentration and the convective flow rate of the POPC-rich phase to vary the concentration distribution with time in the control volume. In Figure 5, the curves in the $N_R-\alpha$ plot obtained from the systems with different initial species concentrations or convection flow rates have very similar initial slopes, indicating that the concentration distribution does not influence the overall amount entering into the raft, and our assumption of first-order kinetics is justified.

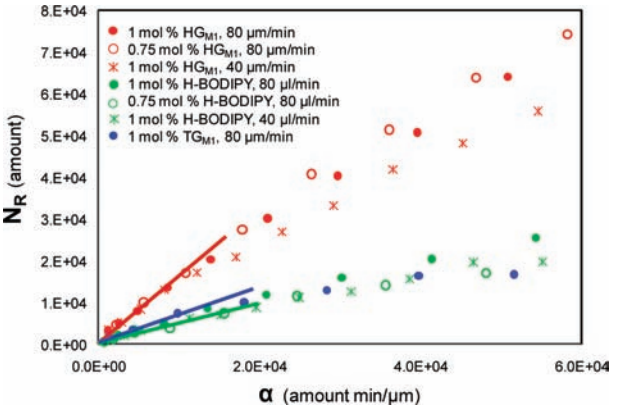

Figure 5. The amount of species in the raft phase region (N_R) as a function of α. In the legend, Alex594-head-labeled G_{M1} (red) = HG_{M1}, BODIPY-tail-labeled G_{M1} (blue) = TG_{M1}, and head-labeled BODIPY-DHPE (green) = H-BODIPY). The initial slopes (indicated by red, blue, or green lines) are k_+ in eq 3. The trend lines from the data of closed circles (1 mol % of the target species, flow rate = 80 μL/min), open circles (0.75 mol % of target species, flow rate = 80 μL/min), and stars (1 mol % of the target species, flow rate = 40 μL/min) are similar, indicating the concentration profile does not influence the association rate constant and the association is first order in concentration. The lines deviate from linear behavior at later times because at later times, the dissociation term and the molar flow rate term, shown in eq 1, started to contribute to the accumulated amount in the raft phase (N_R) and can no longer be neglected.

Dissociation Kinetics Analyses. To obtain the dissociation kinetics information, we essentially reversed the association process by bringing a pristine POPC-rich phase in contact with the raft phase already loaded with target species (following an equilibration step, described in the next section) and tracked their dissociation. This step was accomplished by reversing the hydrodynamic flow and pushing fresh POPC-rich phase bilayer back through the channel. When the concentration in the POPC-rich phase is low, the association term in eq 1 may be neglected. In addition, because we allowed the system to equilibrate with no flow for 2 h before reversing the flow to conduct the dissociation step, the species concentration in the raft was relatively constant in the x-direction in our control volume. In the middle of the channel, we assumed the flow rate of raft phase was relatively constant in the x-direction under the same hydrodynamic force. Therefore, $F_{R,in}$ and $F_{R,out}$ (flow rate times concentration) are similar and the molar flow rate term could be neglected. If we further assume that the dissociation also follows first-order kinetics in concentration at the raft phase interface, we can simplify eq 1

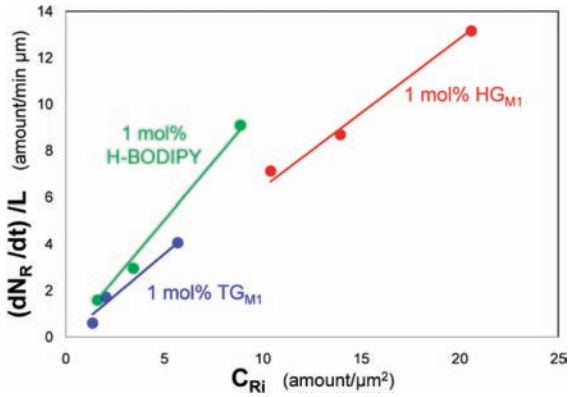

Figure 6. Plot of $(dN_R(t)/dt)/L$ against $C_{Ri}(t)$ to obtain the dissociation rate constant, k_-. The slope of the lines are the k_- for each biomolecule. These values are listed in Table 1. H-BODIPY = head-labeled BODIPY-DHPE (green), TG_{M1} = tail-labeled G_{M1} (blue), HG_{M1} = head-labeled G_{M1} (red).

to eq 5 during the late dissociation stage:

$$\frac{dN_R(t)}{dt} = -\int_{x=0}^{x=L} k_- C_R(x,0,t)dx \quad (5)$$

After our equilibrating stage, the species concentration in the x-direction inside the control volume is relatively uniform. Therefore, we can assume that the concentration is independent of x and eq 5 can be rewritten as:

$$\frac{dN_R(t_d)}{dt} = -k_- C_{Ri}(t_d)L \quad (6)$$

where C_{Ri} represents the species concentration at the interface in the raft phase region, L is the length of the control volume, and t_d is a certain time during the dissociation measurement.

The left term in eq 6 can be obtained from the slope of the dissociation part of N_R-t plot, such as Figure 3a. As for the right term of eq 6, in contrast to the association case, the species concentration is no longer uniform along the y-direction because of the slow diffusion of species in the raft phase so the bulk concentration cannot be used to represent the interface concentration. Therefore, we need to obtain C_{Ri} directly from the intensity profile in the y-direction, as described in detail in the Supporting Information. At different time points during the dissociation stage, we can obtain dN_R/dt and a corresponding C_{Ri} at that time. The dissociation rate constant, k_-, can be obtained from the slope of the plot of $(dN_R(t)/dt)/L$ against $C_{Ri}(t)$, as shown in Figure 6. Note that the data points used to obtain the dissociation rate constant are chosen at the time when the concentration of species is already low in the POPC-rich phase so that the association term can be neglected and eq 6 is valid.

Partition Coefficients. We define our partition coefficient as the ratio of the concentration in the raft phase region over the concentration in the POPC-rich phase region after the system has equilibrated for 2 h, as shown in the left two terms of eq 7:

$$K = \frac{C_R}{C_F} = \frac{k_+}{k_-} \quad (7)$$

At true equilibrium, the concentrations of species in each phase in the system do not change, and at any location at the interface, the rate of species leaving from the raft phase to POPC-rich phase should be equal to the rate of species entering into the raft from the POPC-rich phase at the interface, expressed in eq 8:

$$k_+ C_{Fi} = k_- C_{Ri} \quad (8)$$

Thus, under equilibrium conditions, we can obtain the right two terms of eq 7 by reorganizing eq 8. These equations allow us to obtain K, the partition coefficient at equilibrium, for a target species by two different ways and compare their values.

First, K (eq) was obtained by measuring the relative fluorescence intensity in each phase after equilibrating and taking the ratio of raft concentration to POPC-rich concentration. In separate control experiments, we verified that the intensity of the fluorescence varied linearly with concentration in the range we used and that the fluorescence levels of each biomolecule in the raft and POPC-rich phases were nearly identical (see Supporting Information) so that we could use fluorescence intensity as a proxy for concentration. In the case of head-labeled G_{M1}, the bulk intensities in each phase were nearly uniform across the each phase, up to the interface. However, the raft concentrations of BODIPY-DHPE and tail-labeled G_{M1} are difficult to define because of a suspected disruption effect, described in a later section. Therefore, for these species we used the concentrations of each phase at the phase boundaries with the assumption that the concentrations at the phase boundaries reached local equilibrium. Our definition of the phase boundaries can be found in Supporting Information.

As far as we know, no equilibrium K value based on fluorescence data for head-labeled G_{M1} has been reported in the literature, although previous atomic force microscopy (AFM) study[28] has shown it prefers to partition to liquid-ordered phase over liquid-disordered phase. Only cholera-toxin bound G_{M1} data has been reported, which should be significantly different from head-labeled G_{M1} because the toxin is in a pentamer form and can bind to multiple G_{M1}.[49] The previously reported K (eq) values or the partition preference of tail-labeled G_{M1} has been found to vary significantly from literature to literature. It has been shown to prefer liquid-disordered phase,[27,28] liquid-ordered phase,[23,29] or evenly to both.[23] The discrepancy between these reports indicate that the partition of tail-labeled G_{M1} is probably sensitive to the variation of membrane compositions, which could also be explained by the hypothesized disruption effect, as described in the following section. There are only a few reports examining the "head-labeled" BODIPY-DHPE partitioning preference.[27,50] Plochberger et al. obtained the K (eq) as 0.319,[50] which is comparable to our reported value of 0.6. Chiantia et al. reported the K (eq) as 0.075,[27] which is 1 order of magnitude lower than our value. One reason for the discrepancy is that their low K (eq) value is derived by using the concentration in the bulk raft phase over the concentration in the bulk fluid phase instead of using the local equilibrium concentrations in the two phases at the interfaces.

The second way to obtain the K values is from the ratio of the association/dissociation kinetic parameters, which is valid for first-order kinetics. This second method provides a cross-check for our assumption about the order of kinetics. The values we obtain using this latter method are consistent with the K's obtained directly from the fluorescence intensity data, as summarized in Table 1. This match further supports our assumption of first-order partitioning kinetics that we made to obtain the kinetic parameters initially.

Structure of G_{M1} Influences the Raft Affinity. Tail-labeled G_{M1} shows intrinsic affinity to the raft phase weaker than that of head-labeled G_{M1}.[27,28,51] Head-labeled G_{M1} has the same acyl chains as those for regular G_{M1}, whose carbonyl and amide

Table 1. The Association/Dissociation Rate Constants and Partition Coefficients of Various Membrane-Bound Biomolecules

	k_+ (μm/min)	k_- (μm/min)	K (= k_+/k_-)	K (eq)
head-labeled G_{M1}	1.53 ± 0.03	0.85 ± 0.03	1.8	1.96
head-labeled BODIPY-DHPE	0.57 ± 0.08	0.98 ± 0.04	0.58	0.6
tail-labeled G_{M1}	0.64 ± 0.07	0.72 ± 0.05	0.89	0.75

functional groups can form hydrogen bonds with other sphingolipids and cholesterol.[52] Hydrogen-bonding enhances its association with the raft phase. When G_{M1} is labeled at its tail, the bulky fluorophore can cause steric hindrance, preventing G_{M1} from forming hydrogen bonding with other molecules. These structural distinctions explain differences in overall affinity; here we observe that these differences also impact the kinetics of association, while dissociation is less affected.

As for head-labeled BODIPY-DHPE, literature has reported that it prefers to partition into a disordered phase.[26−28] Although having saturated acyl chains, which might lead to predictions that it would associate with the raft phase over the more disordered POPC-rich phase, it lacks the functional groups to form a hydrogen bonding network with the molecules in the raft phase.[53] Apparently these differences impact BODIPY-DHPE's association with the raft phase significantly and is an interesting point for further study.

Potential Disruption Effects of BODIPY-DHPE and Tail-Labeled G_{M1}. One point of note is that although our data show that BODIPY-DHPE and tail-labeled G_{M1} have low affinity for the raft phase in the time scale of minutes to hours, we observe that over long times, they both gradually penetrate into the raft phase and become almost equally distributed into the predetermined raft region in the time scale of many hours to days (for a 50 μm penetration length). We hypothesize that these molecules gradually start to change the structure of the raft phase, as they penetrate deeper into the raft region. A previous study from Burns et al. also shows evidence that the head-labeled BODIPY-DHPE could disrupt liquid-ordered domains.[28] In addition, some model system studies have reported that the tail-labeled G_{M1} partitions into liquid-disordered phase,[27,28] while others report that they partition to liquid-ordered phase[23,29]or evenly to both liquid-ordered and liquid disordered phases.[23] The discrepancy between these reports could be due to the different membrane compositions used in different model systems, because changing composition, especially cholesterol content, has been shown to significantly change the partition behavior of some fluorescent lipid probes.[37] These phenomena, observed after the system reached equilibrium or a metastable state, support the hypothesis that these molecules could disrupt the lipid rafts and even change lipid raft composition in a longer time scale. In this paper, however, we are more interested in comparing the affinity of the molecules to the raft phase that occurs on a much shorter time scale than the time scale in which the raft structure might be disrupted. Data to support that local equilibrium has been reached over the time scale we are interested in is provided in the Supporting Information, Figure S8. We note that the disruption effect could be further studied by focusing on the data collected on a longer time scale.

Time Scale for Membrane Molecules To Associate/Dissociate with "Lipid Rafts". In this study, the obtained association/dissociation rate constants represent how fast a membrane species passes across a designated interface to/from the raft phase from/to the POPC-rich phase. The current understanding of cell membrane lipid rafts is that they are small (10−200 nm), heterogeneous, highly dynamic, sterol- and sphingolipid-enriched domains, and they can sometimes be stabilized to form large microdomains.[10,11,13] For a membrane molecule to associate with a patch of lipid rafts, it needs to diffuse to the patch, jump across the interface, and diffuse inside the patch. The rate-limiting step(s) determines how fast a molecule can associate and interact with a new phase.

It is possible that the interfacial mass transfer kinetic process across the interface could be the rate-limiting process of the overall association process of a biomolecule with a particular lipid phase under certain conditions. We used fluorescence recovery after photobleaching (FRAP) to measure the diffusivity of Alexa594-head-labeled G_{M1} in both lipid phases separately and found the diffusion coefficients to be 0.77 μm^2/se and 0.06 μm^2/s in the POPC-rich and raft phases, respectively. To make a rough estimate of when this interfacial rate might be limiting, we considered the following scenario. We consider that a G_{M1} molecule must diffuse to a domain with 200 nm size from a location at 1 μm (1/20 of a 20 μm cell size) in the POPC-rich phase away from the domain. The rate for a molecule to diffuse to the interface can be estimated to be 0.77 μm/s (diffusion coefficient/distance). The rate of the molecule to pass across the interface is ~0.025 μm/s (from Table 1), and the diffusion rate from the interface into the middle of the raft patch (~100 nm) is estimated as 0.6 μm/s. These approximate calculations show that the kinetics of molecule passing the interface could play an important role or dominate in the overall association rate of G_{M1} to the raft region. Notice that ideally this method could also be applied to describe the association of a bundle of cross-linked molecules, or membrane molecules with lipid shells after measuring their partitioning kinetics and diffusivity in each phase. It will be interesting to see if crossing the interface is the rate-limiting step for other large membrane biomolecules, which are known to have slower diffusivity.

Note that elevated temperatures above the phase transition point are used when we formed the raft phase bilayer because we found that vesicles below the phase transition temperature are difficult to rupture to form a supported bilayer. It has been reported that the fluid-to-gel phase transition can result in the surface defects in supported lipid bilayers due to the stress induced by the shrinkage of area per phospholipids.[54,55] We found that the gradual cooling and the annealing steps, as described in the Supporting Information, allow the supported raft bilayer to "relax" and presumably maintain its continuity as it shrinks. We did notice that more defects in the raft phase were present when the device was cooled rapidly; however, empirically we determined that our cooling conditions minimized these defects on the microscale (see Supporting Information). We cannot completely exclude the possibilities that there are submicrometer or nanoscale defects in our raft membranes; however, AFM images of the bilayer phases (see Supporting Information) support that the bulk phases are relatively homogeneous and no nanoscale fractured topology exists. Additionally, previous literature reports that defect ratios of lipid membranes going through the fluid-to-gel transition are relatively low (<4%) with an appropriate cooling/annealing process,[54,55] which is similar to what we obtain with our procedure. Using this percentage of defects, our experimental model and the obtained parameters should be still valid within error ranges.

As a final note, we performed our assays within a supported lipid bilayer. It is known that the solid support interaction can influence the lipid mobility in a supported lipid bilayer. In general, the diffusivity of species in supported lipid bilayers is slower than in giant unilamellar vesicles which have free-standing bilayers.[56] It is possible that the rate of species passing the interface is also influenced to the same degree by the support and the rate-limiting step analyses is still valid. In addition, although we do not know how the solid support interaction might influence the absolute number of the association/dissociation rate constants, the relative affinity between different membrane species should still be valid as long as the species does not have specific or direct interaction with the solid support. In the case of glycolipids or lipid-linked proteins, e.g., GPI-linked, this assumption should be valid; however, for transmembrane proteins, to minimize these effects, a cushion or spacing layer (e.g., dextran or polyethylene glycol) could be used to minimize protein−support interactions[57]

Here, we have demonstrated the possibility to construct a predetermined patterned, two-phase coexistent bilayer. The two-phase coexistent compositions we chose were guided by previously published phase diagrams for giant unilamellar vesicles and a hypothetical tie line. The phase diagram in a supported bilayer is likely to be shifted somewhat from the giant unilamellar case;[58] however the compositions we used were found empirically to be two-phase stable for at least 4 h. More stable phase coexistent bilayers may be possible after more accurate phase diagram and tie line information is obtained for supported bilayers systems. It should also be possible to extend this method to test the relative association affinity of biomolecules to different types of physiologically relevant phases with more complicated membrane compositions, as long as the phases are sufficiently stable during the time needed for the assay.

CONCLUSIONS

Herein, we demonstrated a new approach for assaying the partition kinetics of head-labeled G_{M1}, tail-labeled G_{M1}, and head-labeled BODIPY-DHPE in patterned, heterogeneous supported lipid bilayers. We find that these different molecules exhibit significantly different partitioning kinetics to the raft phase tested here. Structural features of these biomolecules, such as label location and the ability to form hydrogen bonds, may influence the partitioning kinetics, especially the association of these molecules to the raft phase, based on our results. Dissociation kinetics from the raft phase are much less variable between these different biomolecules and may indicate that these features have less influence on the dissociation behavior.

The general features of our platform that allow us to make these new kinetic measurements include the control of when a target biomolecule first encounters predetermined and fixed phase locations, which does not require extra labels to distinguish different phases from each other. In this case, we used fluorescent labels only to track our target species and to quantify the amount of species entering/leaving the predefined raft region. In the future, some other surface characterization tools that can measure spatial mass change, such as surface plasma resonance imaging[59] and a quartz crystal microbalance,[60,61] could be coupled to the platform for label-free measurement. In addition, the approach described herein could be extended to assay the partition behavior of other lipids and proteins with posttranslational modifications, such as the addition of GPI anchors, sterols, and single saturated or unsaturated fatty acids, because creating supported bilayers from sections of cell membrane is already possible.[62,63]

Many factors have been suggested to regulate the raft phase association of membrane biomolecules, such as different types of lipid modifications,[64] changes in raft composition,[32,65] chemical exposure,[66] changes in pH/ionic strength,[67] and small molecule binding and cross-linkers.[68] This platform and analysis procedure can be used to test and understand the influence of how structural and environment factors influence molecules' partition kinetics to the raft phase, which may provide insight into how the partition dynamics of cell membrane species can be altered.

ASSOCIATED CONTENT

Supporting Information. Materials, experimental procedures, and data analysis. This material is available free of charge via the Internet at http://pubs.acs.org.

AUTHOR INFORMATION

Corresponding Author
sd386@cornell.edu

ACKNOWLEDGMENT

We thank the NSF (EEC 0824381) and an Innovation Grant from the Institute for Biotechnology and Life Science Technologies at Cornell University for support. We thank Teresa Porri for aiding us with AFM imaging and the use of the AFM in the Nanobiotechnology Center at Cornell University. We thank G. Feigenson and A. Travis for useful comments and discussion.

REFERENCES

(1) Simons, K.; Ikonen, E. *Nature (London, U. K.)* **1997**, *387*, 569–572.
(2) Edidin, M. *Nature Reviews Molecular Cell Biology* **2003**, *4*, 414–418.
(3) Sprenger, R. R.; Horrevoets, J. G. *Proteomics* **2007**, *7*, 2895–2903.
(4) Shaw, A. S. *Nat. Immunol.* **2006**, *7*, 1139–1142.
(5) Zheng, Y. Z.; Foster, L. J. *Proteomics* **2009**, *72*, 12–22.
(6) Simons, K.; Vaz, W. L. C. *Annu. Rev. Biophys. Biomol. Struct.* **2004**, *33*, 269–295.
(7) Pike, L. J. *J. Lipid Res.* **2009**, *50*, S323–S328.
(8) Lingwood, D.; Simons, K. *Science* **2010**, *327*, 46–50.
(9) Simons, K.; Toomre, D. *Nat. Rev. Mol. Cell Biol.* **2000**, *1*, 31–39.
(10) Pike, L. J. *J. Lipid Res.* **2006**, *47*, 1597–1598.
(11) Jacobson, K.; Mouritsen, O. G.; Anderson, R. G. W. *Nat. Cell Biol.* **2007**, *9*, 7–14.
(12) Dietrich, C.; Volovyk, Z. N.; Levi, M.; Thompson, N. L.; Jacobson, K. *Proc. Natl. Acad. Sci.* **2001**, *98*, 10642–10647.
(13) Kenworthy, A. K.; Nichols, B. J.; Remmert, C. L.; Hendrix, G. M.; Kumar, M.; Zimmerberg, J.; Lippincott-Schwartz, J. *J. Cell Biol.* **2004**, *165*, 735–746.
(14) Selvaraj, V.; Buttke, D. E.; Asano, A.; Mcelwee, J. L.; Wolff, C. A.; Nelson, J. L.; Klaus, A. V.; Hunnicutt, G. R.; Travis, A. J. *J. Androl.* **2007**, *28*, 588–599.
(15) Chazal, N.; Gerlier, D. *Microbiol. Mol. Biol. Rev.* **2003**, *67*, 226–237.
(16) Cordy, J. M.; Hooper, N. M.; Turner, A. J. *Mol. Membr. Biol.* **2006**, *23*, 111–122.
(17) Ohno-Iwashita, Y.; Shimada, Y.; Hayashi, M.; Inomata, M. *Geriatr. Gerontol. Int.* **2010**, *10*, S41–S52.

(18) Fulop, T.; Larbi, A.; Dupuis, G.; Pawelec, G. *Arthritis Res. Ther.* **2003**, *5*, 290–302.
(19) Munro, S. *Cell* **2003**, *115*, 377–388.
(20) Carvalho, K.; Ramos, L.; Roy, C.; Picart, C. *Biophys. J.* **2008**, *95*, 4348–4360.
(21) Dietrich, C.; Volovyk, Z. N.; Levi, M.; Thompson, N. L.; Jacobson, K. *Proc. Natl. Acad. Sci. U.S.A.* **2001**, *98*, 10642–10647.
(22) Hammond, A. T.; Heberle, F. A.; Baumgart, T.; Holowka, D.; Baird, B.; Feigenson, G. W. *Proc. Natl. Acad. Sci. U.S.A.* **2005**, *102*, 6320–6325.
(23) Sengupta, P.; Hammond, A.; Holowka, D.; Baird, B. *Biochim. Biophys. Acta* **2008**, *1778*, 20–32.
(24) Levental, I.; Lingwood, D.; Grzybek, M.; Coskun, N.; Simons, K. *Proc. Natl. Acad. Sci. U.S.A.* **2010**, *107*, 22050–22054.
(25) Morales-Penningston, N. F.; Wu, J.; Farkas, E. R.; Goh, S. L.; Konyakhina, T. M.; Zheng, J. Y.; Webb, W. W.; Feigenson, G. W. *Biochim. Biophys. Acta* **2010**, *1798*, 1324–1332.
(26) Baumgart, T.; Hunt, G.; Farkas, E. R.; Webb, W. W.; Feigenson, G. W. *Biochim. Biophys. Acta* **2007**, *1768*, 2182–2194.
(27) Chiantia, S.; Ries, J.; Kahya, N.; Schwille, P. *ChemPhysChem* **2006**, *7*, 2409–2418.
(28) Burns, A. R.; Frankel, D. J.; Buranda, T. *Biophys. J.* **2005**, *89*, 1081–1093.
(29) Wang, T.-Y.; Leventis, R.; Silvius, J. R. *Biophys. J.* **2000**, *79*, 919–933.
(30) Mishra, S.; Joshi, P. G. *J. Neurochem.* **2007**, *103*, 135–142.
(31) Sachs, J. N.; Engelman, D. M. *Annu. Rev. Biochem.* **2006**, *75*, 707–712.
(32) Wong, W.; Schlichter, L. *J. Biol. Chem.* **2003**, *279*, 444–452.
(33) He, H.-T.; Marguet, D. *Annu. Rev. Phys. Chem.* **2011**, *62*, 417–436.
(34) Blanchette Craig, D.; Lin, W.-C.; Ratto Timothy, V.; Longo Marjorie, L. *Biophys. J.* **2006**, *90*, 4466–4478.
(35) Lin, W.-C.; Blanchette, C. D.; Ratto, T. V.; Longo, M. L. *Methods Membr. Lipids* **2007**, 503–513.
(36) Bagatolli, L. A. *Biochim. Biophys. Acta* **2006**, *1758*, 1541–1556.
(37) Crane, J. M.; Tamm, L. K. *Biophys. J.* **2004**, *86*, 2965–2979.
(38) Groves, J. T.; Dustin, M. L. *J. Immunol. Methods* **2003**, *278*, 19–32.
(39) Richter, R. P.; Him, J. L. K.; Brisson, A. *Mater. Today (Oxford, U. K.)* **2003**, *6*, 32–37.
(40) Sackmann, E. *Science (Washington, D. C.)* **1996**, *271*, 43–48.
(41) Chao, L.; Gast, A. P.; Hatton, T. A.; Jensen, K. F. *Langmuir* **2009**, *26*, 344–356.
(42) Daniel, S.; Diaz, A. J.; Martinez, K. M.; Bench, B. J.; Albertorio, F.; Cremer, P. S. *J. Am. Chem. Soc.* **2007**, *129*, 8072–8073.
(43) Simons, K.; Vaz, W. L. C. *Annu. Rev. Biophys. Biomol. Struct.* **2004**, *33*, 269–295.
(44) Veatch, S. L.; Keller, S. L. *Phys. Rev. Lett.* **2005**, *94*, 148101.
(45) Kam, L.; Boxer, S. G. *J. Am. Chem. Soc.* **2000**, *122*, 12901–12902.
(46) Leonenko, Z. V.; Carnini, A.; Cramb, D. T. *Biochim. Biophys. Acta* **2000**, *1509*, 131–147.
(47) Jonsson, P.; Beech, J. P.; Tegenfeldt, J. O.; Hook, F. *J. Am. Chem. Soc.* **2009**, *131*, 5294–5297.
(48) Wegner, G. J.; Wark, A. W.; Lee, H. J.; Codner, E.; Saeki, T.; Fang, S.; Corn, R. M. *Anal. Chem.* **2004**, *76*, 5677–5684.
(49) Merritt, E. A.; Sarfaty, S.; Akker, F. V. D.; L'Hoir, C.; Martial, J. A.; Hol, W. G. J. *Protein Sci.* **1994**, *3*, 166–175.
(50) Plochberger, B.; Stockner, T.; Chiantia, S.; Brameshuber, M.; Weghuber, J.; Hermetter, A.; Schwille, P.; Schutz, G. J. *Langmuir* **2010**, *26*, 17322–17329.
(51) Wang, T.-Y.; Silvius, J. R. *Biophys. J.* **2003**, *84*, 367–378.
(52) Barenholz, Y.; Thompson, T. E. *Biochim. Biophys. Acta* **1980**, *604*, 129–158.
(53) Ramstedt, B.; Slotte, J. P. *Biochim. Biophys. Acta* **2006**, *1758*, 1945–1956.
(54) Xie, A. F.; Yamada, R.; Gewirth, A. A.; Granick, S. *Phys. Rev. Lett.* **2002**, *89*, 246103.
(55) Charrier, A.; Thibaudau, F. *Biophys. J.* **2005**, *89*, 1094–1101.
(56) Przybylo, M.; Sykora, J.; Humpolíková, J.; Benda, A.; Zan, A.; Hof, M. *Langmuir* **2006**, *22*, 9096–9099.
(57) Tanaka, M.; Rossetti, F. F.; Kaufmann, S. *Biointerphases* **2008**, *3*, FA12–FA16.
(58) Tokumasu, F.; Jin, A. J.; Feigenson, G. W.; Dvorak, J. A. *Biophys. J.* **2003**, *84*, 1–10.
(59) Nelson, B. P.; Grimsrud, T. E.; Liles, M. R.; Goodman, R. M.; Corn, R. M. *Anal. Chem.* **2000**, *73*, 1–7.
(60) Ebara, Y.; Okahata, Y. *J. Am. Chem. Soc.* **1994**, *116*, 11209–11212.
(61) Keller, C. A.; Kasemo, B. *Biophys. J.* **1998**, *75*, 1397–1402.
(62) Dodd, C. E.; Johnson, B. R. G.; Jeuken, L. J. C.; Bugg, T. D. H.; Bushby, R. J.; Evans, S. D. *Biointerphases* **2008**, *3*, FA59–FA67.
(63) Frankel, D. J.; Pfeiffer, J. R.; Surviladze, Z.; Johnson, A. E.; Oliver, J. M.; Wilson, B. S.; Burns, A. R. *Biophys. J.* **2006**, *90*, 2404–2413.
(64) Lopez-Montero, I.; Monroy, F.; Velez, M.; Devaux, P. F. *Biochim. Biophys. Acta* **2010**, *1798*, 1348–1356.
(65) Tikku, S.; Epshtein, Y.; Collins, H.; Travis, A. J.; Rothblat, G. H.; Levitan, I. *Am. J. Physiol. Cell Physiol.* **2007**, *293*, 440–450.
(66) Dolganiuc, A.; Bakis, G.; Kodys, K.; Mandrekar, P.; Szabo, G. *Alcoholism: Clin. Exp. Res.* **2006**, *30*, 76–85.
(67) Hartmann, W.; Galla, H. J.; Sackmann, E. *FEBS Lett.* **1977**, *78*, 169–172.
(68) Kahya, N.; Brown, D. A.; Schwille, P. *Biochemistry* **2005**, *44*, 7479–7489.